

SEISMIC INTERFEROMETRY BY DECONVOLUTION: THEORY AND EXAMPLES

IVAN VASCONCELOS and ROEL SNIEDER
Center for Wave Phenomena, Colorado School of Mines, Golden CO 80401, USA

Abstract

Seismic interferometry is a field of growing interest in exploration seismology. In this paper we provide the theoretical basis for performing interferometry by deconvolution. We argue that for arbitrarily complicated models, deconvolution interferometry gives the causal scattering response between any two receivers. Interferometry by cross-correlation, on the other hand, gives both causal and acausal scattering responses. Even with a closed surface of integration, deconvolution interferometry also gives rise to spurious events not present in its cross-correlation counterpart. These events arise from an extra boundary condition which is imposed by the deconvolution method in interferometry. We demonstrate the feasibility of deconvolution interferometry with numerical examples with impulsive sources, and show that the deconvolution interferometry artifacts typically are not mapped onto the image space. One application that can potentially benefit from deconvolution interferometry is imaging from drill-bit noise recordings. We compare the results from deconvolution interferometry to cross-correlation interferometry in numerical examples for a single-layer case and a subsalt drill-bit imaging example.

Introduction

Conventional seismic interferometry consists in extracting the Green's function between two receivers by correlating the wavefields excited by incoherent sources and recorded at these two receivers (e.g., Weaver and Lobkis, 2004). Our objective here is to demonstrate that by deconvolving one recorded wavefield with the other, one can also extract the response between the receivers.

Interferometry by cross-correlation is also known to preserve characteristics of the input excitation (e.g., the power spectrum of the source function). Deconvolution interferometry could then be a preferred method for cases in which the recorded data was excited by a complicated and poorly-known function. One example of this is drill-bit noise processing, where cross-correlated drill-bit noise shows a strong imprint of the drill-bit source function (Poletto and Miranda 2004). If this source imprint is not accounted for, the resulting drill-bit noise image could be uninterpretable. Deconvolution interferometry can not only be a viable option to interferometric imaging, but it may also prove to be a key technology in some applications, such as imaging from drill-bit noise.

Deconvolution interferometry

Let the frequency-domain wavefield $u(\mathbf{r}_A, \mathbf{s}, \omega)$ recorded at \mathbf{r}_A be the superposition of an unperturbed wavefield and a wavefield perturbation, represented respectively by $u_0(\mathbf{r}_A, \mathbf{s}, \omega)$ and $u_S(\mathbf{r}_A, \mathbf{s}, \omega)$. The source function is given by $S_s(\omega)$, associated with an excitation at \mathbf{s} . It is important to note here that the medium may be arbitrarily heterogeneous and anisotropic, and that the recorded wavefields may contain higher-order scattering and inhomogeneous waves. Also, $S_s(\omega)$ can have a complicated character, and may vary as a function of \mathbf{s} . Given that the deconvolution of a wavefield recorded at \mathbf{r}_A by that recorded at \mathbf{r}_B is represented by D_{AB} , then to perform interferometry by deconvolution it is necessary to integrate D_{AB} over a closed surface Σ containing the sources:

$$\int_{\Sigma} D_{AB}(\omega) d\mathbf{s} = \int_{\Sigma} \frac{u(\mathbf{r}_A, \mathbf{s}, \omega) u^*(\mathbf{r}_B, \mathbf{s}, \omega)}{|u(\mathbf{r}_B, \mathbf{s}, \omega)|^2} d\mathbf{s}, \quad (1)$$

where $*$ denotes complex-conjugation. We can see from right-hand side of equation [1] that the source function $S_s(\omega)$ cancels in the integrand. As in the cross-correlation approach (Snieder et al., 2006), the numerator in equation [1] is not zero-phase whereas the denominator is strictly zero-phase, but it is oscillatory and contains cross-terms between the scattered and direct wavefields recorded at \mathbf{r}_B . To evaluate the integral in equation [1], we expand the integrand in a power series. In this expansion, we identify the most prominent terms in the expansion of equation [1] by assuming $|u_0|^2 \gg |u_S|^2$ to drop terms which

are quadratic on scattered wavefield. This approximation is analogous to the Born approximation for the Lippmann-Schwinger scattering series. From the series expansion of the integrand on the right-hand side of equation [1], the terms that are of leading order in the scattered wavefield are

$$\int_{\Sigma} D_{AB}(\omega) ds = \underbrace{\int_{\Sigma} \frac{u_0(\mathbf{r}_A, \mathbf{s}, \omega) u_0^*(\mathbf{r}_B, \mathbf{s}, \omega)}{|u_0(\mathbf{r}_B, \mathbf{s}, \omega)|^2} ds}_{D1} + \underbrace{\int_{\Sigma} \frac{u_S(\mathbf{r}_A, \mathbf{s}, \omega) u_0^*(\mathbf{r}_B, \mathbf{s}, \omega)}{|u_0(\mathbf{r}_B, \mathbf{s}, \omega)|^2} ds}_{D2} - \underbrace{\int_{\Sigma} \frac{u_S(\mathbf{r}_B, \mathbf{s}, \omega) u_0(\mathbf{r}_A, \mathbf{s}, \omega) u_0^*(\mathbf{r}_B, \mathbf{s}, \omega)}{u_0(\mathbf{r}_B, \mathbf{s}, \omega)} ds}_{D3}. \quad (2)$$

For most practical applications, $u_0(\mathbf{r}_B, \mathbf{s}, \omega)$ is slowly varying and the oscillatory character of integrands in $D1$ and $D2$ (equation [2]) is mostly controlled by their numerators.

To understand the physics behind the terms in equation [2], it is useful at this point to review interferometry by cross-correlation:

$$\int_{\Sigma} C_{AB}(\omega) ds = \int_{\Sigma} |S_s(\omega)|^2 u(\mathbf{r}_A, \mathbf{s}, \omega) u^*(\mathbf{r}_B, \mathbf{s}, \omega) ds \approx |S(\omega)|^2 (C1 + C2 + C3 + C4), \quad (3)$$

where $C_{AB}(\omega)$ is the cross-correlation between the wavefields measured at \mathbf{r}_A and \mathbf{r}_B , excited by a source at \mathbf{s} . $|S(\omega)|^2$ is the power spectrum of $S_s(\omega)$ (for simplicity, we assume here the source is the same at all shots). The terms $C1$ through $C4$ arise from the cross-terms in the integrand of equation [3]. In correlation interferometry, the term $C2$ gives rise to a causal response corresponding to $u_S(\mathbf{r}_A, \mathbf{r}_B, \omega)$, which is the scattered wavefield as if the source were located at \mathbf{r}_B . $C3$ gives a response that corresponds to $u_S^*(\mathbf{r}_A, \mathbf{r}_B, \omega)$. The terms $C1$ and $C4$ are respectively associated with causal and acausal $u_0(\mathbf{r}_A, \mathbf{r}_B, \omega)$. Snieder et al. (2006) verify this interpretation by analytically studying interferometry terms for direct and primary-reflected waves.

The phase in the integrand of $D1$ (equation [2]) is equal to that of $C1$ in equation [3]. The same relationship holds between $D2$ and $C2$. $C3$ and $C4$ have no corresponding terms in equation [2]. This remark has an important consequence: interferometry by deconvolution of receiver gathers only provides the causal scattering response as if the excitation occurred at the location of the receiver that acts as the deconvolution filter. Because the wavefields u_0 in the term $D1$ satisfy wave-equations, $D1$ yields both the causal and acausal responses between the receivers for an unperturbed medium (e.g., causal and acausal direct waves). This holds regardless of medium properties or acquisition geometry. It also holds if integration over sources is not conducted over a closed surface, as long as there are sources that lie in the stationary path connecting the integration surface, the receivers and the target scatterers. This interpretation is analogous to the asymptotic interpretation of the terms in cross-correlation interferometry conducted by Snieder et al. (2006).

The term $D3$ in equation [2] gives rise to a spurious event that does not correspond to any physical phenomena that would occur if there were a physical source sitting at one of the receiver locations. The minus sign in front of $D3$ in equation [2] shows that this term will appear with a polarity that is opposite with respect to the other two terms. We will cover the physical significance of this term in our analysis of the single-layer numerical example.

Single-layer model

The model used for the examples portrayed here was composed of a water layer with a wavespeed of 1500 m/s. A flat, horizontal interface was placed at 2500 m depth. The receivers were positioned in a horizontal line at 750 m depth, starting at lateral position $x = 1500$ m and ending at 3000 m, with increments of 25 m. The source line was also horizontal at a depth of 400 m, ranging from $x = 500$ m to 4500 m, with increments of 50 m. The data was modeled by 2D acoustic finite-differencing with absorbing boundary conditions.

Figure 1a,c show deconvolution and cross-correlation gathers computed from the last and first (used as filter) receiver gathers. Figure 1a confirms the presence of the leading order terms highlighted in equation [2], and it is supported by the ray-theoretical traveltimes for the three terms. The acausal $C3$ term and the $C4$, seen in Figures 1c,d indeed are not present in the deconvolution gathers.

The interferometric (virtual) shot gathers for deconvolution before source stack and cross-correlation are shown in Figure 2a and c. Causal and acausal direct arrivals can be seen in both gathers. The causal primary reflection event can also be identified in both gathers. The acausal primary is only present in the correlation gather (c). The spurious event introduced by the term $D3$ (equation [2]; Figure 1a,b) appears in Figure 2, with the same zero-offset traveltime as the primary reflection, but with opposite polarity and with a slower move-out character. Since deconvolution interferometry strictly requires the zero-offset trace to be a spike at $t = 0$ s (Figures 2a,c) and zero at all other times, spurious events with opposite polarity are generated to cancel the contribution of physical events at the zero-offset trace for non-zero times.

The images obtained from shot-profile wave-equation migration the interferometric shot gathers are shown in Figure 2b and d. Both images map the energy at the correct subsurface locations. The similarity between both images shows that the spurious event ($D3$) in Figure 2a vanishes in the image domain. This happens because the imaged depth of the spurious arrival varies with source-receiver offset. Hence, in the stacking of images from different offsets the contribution of deconvolution-driven spurious events add destructively in the final image, whereas primary reflections add constructively.

Imaging with drill-bit noise

Drill-bit noise records are characterized by a continuous noise source that is dominated by certain specific frequencies (Poletto and Miranda, 2004). In typical drill-bit imaging this problem is overcome by placing accelerometers on the drill-stem to estimate the drill-bit source function. Deconvolution interferometry provides a new option to the processing of drill-bit seismic data, specially if the accelerometer records are not available, or if they do not provide a good estimate of the drill-bit excitation. Such a situation may occur with PDC bits (Poletto and Miranda, 2004), commonly used in subsalt drilling.

Using the Sigsbee velocity model, we devised a numerical experiment to simulate drill-bit recordings measured at a subsalt instrumented well. Figure 3a shows the geometry for this experiment which consists of vertical drilling and of an instrumented deviated well with 100 receivers placed every 30 meters. We purposefully chose to record the noise from a drilling well to the left of the recording well to sample the stationary arrivals that bounce off the salt structure. The 60-second long source function (not shown) was modeled after a physical model for a PDC bit excitation from Poletto and Miranda (2004). In this case the image obtained from the synthetization of drill-bit noise with deconvolution interferometry is able to suppress the effect of the source function, giving an impulsive image and even providing some illumination of the subsalt sediments from below (Figure 3b). The imaging from cross-correlation interferometry is of poorer quality because it does not compensate for the effects of the drill-bit source function.

Conclusions

By representing recorded wavefields as a superposition of direct and scattered wavefields, we derived the leading-order terms that follow from performing deconvolution interferometry on receiver gathers before summing over sources. This derivation suggests that interferometry by deconvolution before stacking over sources yields only the causal term related to the scattered wavefield as if one of the receivers were a virtual source. Spurious terms arise in deconvolution interferometry, due to an extra boundary condition imposed by the method.

The single-layer model data showed deconvolution interferometry can successfully retrieve the causal response between two receivers. Imaging of deconvolution interferometric shot gathers proved to practically eliminate the spurious arrivals generated by the deconvolution method. In the Sigsbee subsalt example with a drill-bit source, deconvolution interferometry proved to be able to properly image the subsurface structure without the need for an independent estimate of the source pulse (e.g., drill-stem accelerometer).

References

- Poletto, F., and Miranda, F., 2004, *Seismic While Drilling - Fundamentals of Drill-Bit Seismic for Exploration*: Monograph, Elsevier Ltd., United Kingdom, 520 pages.
- Sniieder, R., Wapenaar, K. and Larner, K., 2006, Spurious multiples in seismic interferometry of primaries: *Geophysics*, **78**, SI111-SI124.
- Weaver, R. L. and Lobkis, O. I., 2004, Diffuse fields in open systems and the emergence of the Green's function: *J. Acoust. Soc. Am.*, **116**,2731–2734.

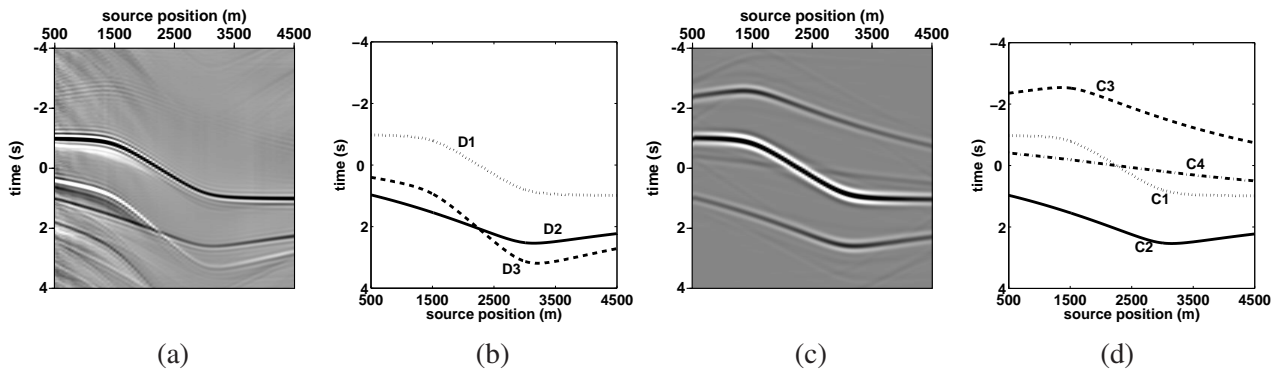


Figure 1: Deconvolution and cross-correlation gathers for the first and last receivers, whose lateral positions are, respectively, 1500 and 3000 m. (a) displays the deconvolution gather obtained from deconvolving the modeled common-receiver gathers, whereas (b) shows ray-theoretical traveltimes for the terms in equation [2]. Analogous to (a), (b) is the cross-correlation gather generated from source-by-source correlation of the two receiver gathers. (c) shows the asymptotic traveltimes corresponding to the phase of the integrands in equation [3].

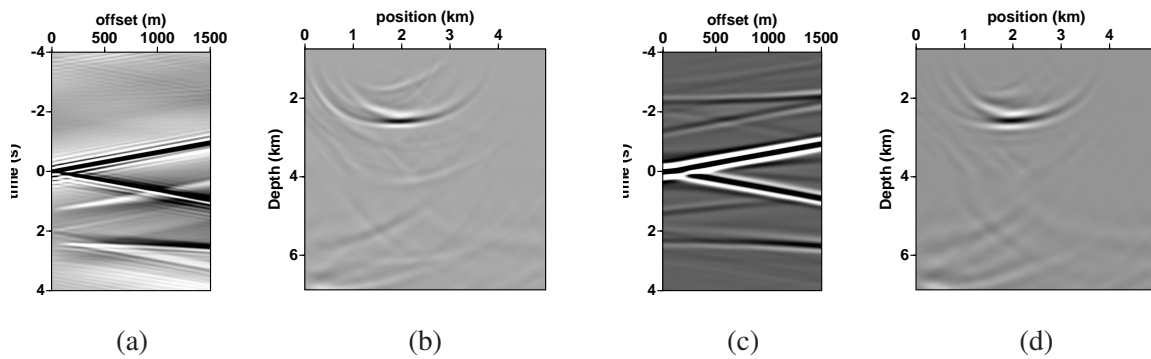


Figure 2: Virtual (interferometric) shot gathers with the virtual shot positioned at the receiver at 1500 m. The gather in (a) is obtained by deconvolution before stacking (equation [1]), (c) is generated by cross-correlations (equation [3]). In this figure, (b) and (d) are the images obtained from migrating the gathers in (a) and (c), respectively. The true depth of the target interface is 2500 m.

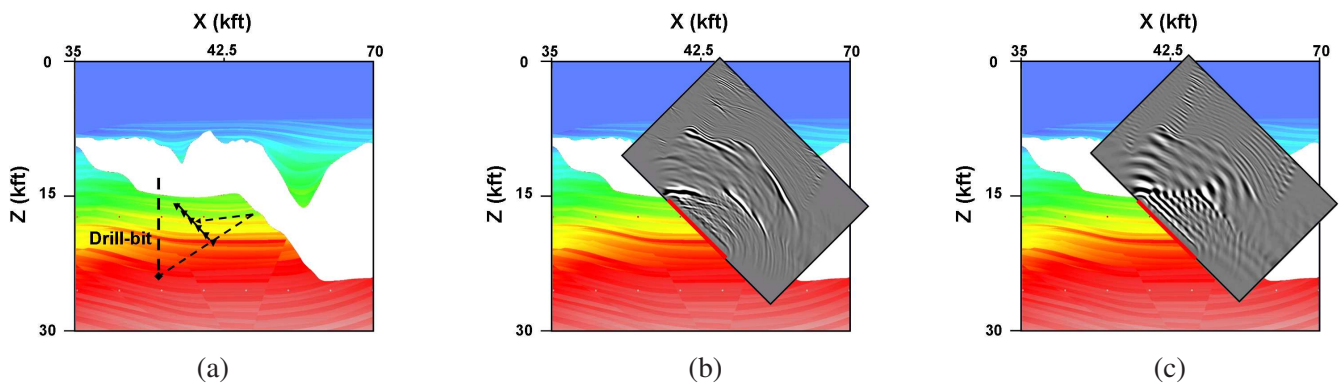


Figure 3: Numerical subsalt drill-bit experiment with the Sigsbee model. The drill-bit geometry is shown by the thick vertical dashed line in (a), whereas the solid line with triangles shows the location of the receiver array. The thin dashed arrow in (a) illustrates a wavepath that would constitute a stationary arrival in the interferometric gathers. The image obtained by deconvolution interferometry is shown in (b), overlaid in the velocity model. (c) is an overlay of the image from cross-correlation interferometry.